UC Office of the President

Title
Modeling Thermal-Hydrologic Processes for a Heated Fractured Rock System: Impact of a Capillary-Pressure Maximum

Permalink
https://escholarship.org/uc/item/6gh0s279

Journal
Transport in Porous Media, 83(3)

ISSN
1573-1634

Authors
Sun, Y.
Buscheck, T. A.
Lee, K. H.
et al.

Publication Date
2010-07-01

DOI
10.1007/s11242-009-9459-1

Peer reviewed

Modeling Thermal-Hydrologic Processes for a Heated Fractured Rock System: Impact of a Capillary-Pressure Maximum

Y. Sun · T. A. Buscheck · K. H. Lee · Y. Hao · S. C. James

Abstract   Various thermal-hydrologic models have been developed to simulate thermal-hydrologic conditions in emplacement drifts and surrounding host rock for the proposed high-level nuclear waste repository at Yucca Mountain, Nevada. The modeling involves two-phase (liquid and gas) and two-component (water and air) transport in a fractured-rock system, which is conceptualized as a dual-permeability medium. Simulated hydrologic processes depend upon calibrated system parameters, such as the van Genuchten α and m, which quantify the capillary properties of the fractures and rock matrix. Typically, these parameters are not calibrated for strongly heat-driven conditions, i.e., conditions for which boiling and rock dryout occur. The objective of this study is to modify the relationship between capillary pressure and saturation, $P_c(S)$, for strongly heated conditions that drive saturation below the residual saturation ($S \rightarrow 0$). We offer various extensions to the van Genuchten capillary-pressure function and compare results from a thermal-hydrologic model with data collected during the Drift-Scale Test, an in situ thermal test at Yucca Mountain, to investigate the suitability of these various P_c extension methods. The study suggests that the use of extension methods and the imposition of a capillary-pressure cap (or maximum) improve the agreement between Drift-Scale Test data and model results for strongly heat-driven conditions. However, for thermal-hydrologic models of the Yucca Mountain nuclear waste repository, temperature and relative humidity are insensitive to the choice of extension method for the capillary-pressure function. Therefore, the choice of extension method applied to models of drift-scale thermal-hydrologic behavior at Yucca Mountain can be made on the basis of numerical performance.

Keywords   Capillary pressure · van Genuchten · Transition saturation · Thermal-hydrology · Repository

Y. Sun · T. A. Buscheck (✉) · K. H. Lee · Y. Hao
Lawrence Livermore National Laboratory, Livermore, CA 94550, USA
e-mail: buscheck1@llnl.gov

S. C. James
Sandia National Laboratories, Livermore, CA 94551, USA

1 Introduction

Radioactive heat of decay from waste packages emplaced in drifts (tunnels) in the proposed high-level nuclear waste repository at Yucca Mountain results in strongly heat-driven conditions, involving boiling, vapor flow, condensation, and condensate flow. Strongly heat-driven conditions cause dryout of the host rock, affecting the thermal-hydrologic environment within the emplacement drifts. Buscheck et al. (2002) developed the MultiScale ThermoHydrologic Model (MSTHM) to predict the range of thermal-hydrologic conditions within emplacement drifts, in the adjoining host rock, and across the entire Yucca Mountain repository (Buscheck et al. 2006; SNL 2007). The MSTHM calculates thermal-hydrologic variables, such as temperature, gas-phase pressure, saturation, evaporation/condensation rates, etc. Engineered design parameters, such as drift and waste-package spacing and waste-package heat generation rate, and natural-system parameters, such as percolation flux and thermal-hydrologic properties in the host rock, are all important to system-wide thermal-hydrologic behavior (SNL 2007).

The sensitivity of thermal-hydrologic variables to host-rock thermal-hydrologic property uncertainty and variability has been studied for the Yucca Mountain nuclear waste repository (Glascoe et al. 2004; Sun et al. 2006; Buscheck et al. 2006). Although the impact of the specific capillary-pressure relation when calculating overall site response appears to be small based on previous parameter-sensitivity studies (Buscheck et al. 2006), the choice of extension to capillary-pressure relation on local temperature and saturation has yet to be addressed in detail.

Residual saturation is usually defined as the saturation level below which fluid drainage under natural conditions will not occur (the effective permeability would be zero). In practice, the residual saturation is often measured in an experiment under room temperature. In previous research, capillary pressure is assumed to increase indefinitely as saturation approaches the residual value (Nitao and Bear 1996). However, under strongly heat-driven conditions, saturation may be reduced below this theoretical limit. Subject to an excessive capillary pressure, the boiling point would increase to a non-physical value because of the vapor-pressure lowering. Under strongly heat-driven conditions, capillary pressure does not go to infinity at *residual saturation*; instead, capillary pressure should have a reasonable upper bound as saturation approaches zero (Webb 2000; Li and Horne 2005). Although several capillary-pressure relationships are available, the van Genuchten (1980) formulation is most widely used because its few parameters are easily fit to experimental data. Similar to other relationships (Brooks and Corey 1996; Luckner et al. 1989), the van Genuchten (1980) relation may need to be modified for strongly heat-driven conditions below residual saturation. In order to apply those relation equations over the full range of saturation from zero to one, a physically reasonable extension (non-asymptotic) to saturations below residual is needed. For both physical and computational reasons, it is preferred that the capillary-pressure versus saturation relation does not have a discontinuity in slope.

Webb (2000) reviewed the modification methods for extending capillary-pressure relations below residual saturation; these and subsequent methods are listed in Table 1.

Since Ross et al. (1991) recalibrated the Campbell (1974) equation to strongly heat-driven conditions using the power law method with a CPC (10^9 Pa), several methods including power laws and linear or exponential functions have been applied to extend capillary-pressure relations to low saturations both with and without recalibration of the capillary-pressure parameters. For example, Webb (2000) proposed a simple exponential extension without recalibration and Spycher et al. (2003) applied a linear extension to avoid numerical difficulties associated with the extremely high capillary pressure.

Table 1 Extension methods of capillary pressure curves

	Reference	Capillary-pressure curve	Extension method
1	Ross et al. (1991)	Campbell (1974)	Power function
2	Campbell and Shiozawa (1992)	van Genuchten (1980)	Exponential function
3	Rossi and Nimmo (1994)	Brooks and Corey (1996)	Power function
			Exponential function
4	Nitao (1998)	Brooks and Corey (1996)	Linear function
		van Genuchten (1980)	
5	Finsterle (2002)	Brooks and Corey (1996)	Linear function
		van Genuchten (1980)	Flat cap value
6	Spycher et al. (2003)	van Genuchten (1980)	Linear function
7	Morel-Seytoux and Nimmo (1999)	Brooks and Corey (1996)	Exponential function
		Rossi and Nimmo (1994)	
8	Webb (2000)	van Genuchten (1980)	Exponential function
9	Nieber et al. (2005)	Brooks and Corey (1996)	Exponential function
10	Khlosi etal. (2006)	Kosugi (1999)	Adsorption equation
			Campbell and Shiozawa (1992)

For the Yucca Mountain Project, data from desaturation experiments under ambient conditions (Flint 1998) are used to calibrate van Genuchten parameters α and m (Zhou et al. 2003). In order to apply van Genuchten parameters to strongly heat-driven conditions relevant to the Yucca Mountain nuclear waste repository, a reasonable extension of the capillary-pressure relation is worth investigating. In particular, it is useful to determine whether such extensions would have an impact on simulated temperatures and relative humidities across the Yucca Mountain repository.

To our knowledge, capillary-pressure extension methods have not been studied in a systematic manner to interpret thermal-hydrologic behavior. In order to avoid recalibration efforts for van Genuchten parameters over the entire saturation range, we prefer to use the originally calibrated parameters in the *wet* region and to apply simple extensions in the *dry* region. Here, we define a *transition saturation*, S_j, that divides the dry and wet saturation regions. Simulations with a flat capillary-pressure cap (CPC) in the dry region are computationally expensive because of the slope discontinuity in the capillary pressure as a function of saturation, $P_c(S)$. When using an exponential extension, the dry region is much wider (and S_j larger) than that from a linear or flat extension. A wider wet region is preferred because it is defined with a calibrated, physics-based relation. Although extension of capillary curves into the dry region improves numerical performance by avoiding extremely high capillary pressures, such methods may be case specific. Further insights into the physical mechanisms and impacts of extension methods are necessary. In this work, we investigate the influence of various extension methods on simulated thermal-hydrologic behavior and conclude that a linear extension with a CPC reasonably represents strongly heat-driven conditions at Yucca Mountain, with relatively low computational effort.

2 Capillary-Pressure Curve Extension Methods

The van Genuchten (1980) function describing the relation between capillary pressure and saturation has been successfully used in flow models at moderate to high saturations; however,

the singularity in the van Genuchten function can be problematic when applied to strongly heat-driven systems. For example, data from the Drift-Scale Test (DST), an in situ thermal test at Yucca Mountain (SNL 2007), demonstrate that when temperatures remain above boiling for a long time, the host rock around the heated drift is completely dried. In order to better represent strongly heat-driven thermal-hydrologic behavior between zero and residual saturation, it may be necessary to apply an extension method to modify the van Genuchten retention curve specified for ambient conditions.

The relation between capillary pressure and saturation is (van Genuchten 1980):

$$P_c = \frac{1}{\alpha} \left(S_e^{-\frac{1}{m}} - 1 \right)^{\frac{1}{n}}, \quad S_e = \frac{S - S_r}{S_m - S_r}, \tag{1}$$

where α [Pa^{-1}] and m [$-$] are curve-fitting parameters, $n = 1/(1 - m)$, and S_e, S_r, and S_m are effective, residual, and maximum saturations, respectively. For a given porosity, the saturation is calculated using volumetric water content. Note that the calibrated van Genuchten curves are valid in the saturation range from S_r to S_m. However, for saturation less than residual saturation ($S < S_r$), there is a pressure singularity $P_c \to \infty$ when $S_e \to 0$. Equation 1 is used for both fracture and matrix continua in dual-permeability models. Because of the small fracture porosity (and small residual saturation in the fractures), we considered it unnecessary to investigate $P_c(S)$ extension for the fracture continuum; therefore, extensions of capillary-pressure curves are only considered for the matrix. Ideally, the maximum capillary pressure should be identified by fitting the $P_c(S)$ curve over the entire saturation domain for each rock material and under a specific thermal condition. In the literature, the maximum P_c value at zero liquid saturation ranges from 1.5×10^6 (Fayer and Simmon 1995) to 10^9 (Ross et al. 1991; Webb 2000). Because of the lack of experimental data in the dry region ($S < S_r$), the maximum P_c value is assumed to be 10^8 Pa in this study.

Various methods are proposed in Table 2 and Fig. 1 to extend the van Genuchten capillary-pressure curve below S_r. The impacts of these methods on simulated thermal-hydrologic behavior are analyzed. In order to keep this article compact, acronyms of extension methods are used throughout.

2.1 Flat Capillary-Pressure Extension (FCPC)

The simplest extension methods of the van Genuchten capillary-pressure curve is a flat (FCPC) curve, which assigns a constant CPC in the dry region (Finsterle 2002; Kolditz and De Jonge 2004) and follows the van Genuchten curve in the wet region (curve ABE of Fig. 1a)

Table 2 Extension methods

	Extension method	Acronym	Curve in Fig. 1
0	**N**o **E**xtension **V**an **G**enuchten	NEVG	VBE (a), VGE (b)
1	**F**lat extension with **CPC**	FCPC	ABE (a)
2	**E**xponential extension with **CPC**	ECPC	ADE (a)
3	**L**inear extension *without* **CPC**	LNOC	FGE (b)
4	**L**inear extension with **CPC**	LCPC	ACE (a)(b)

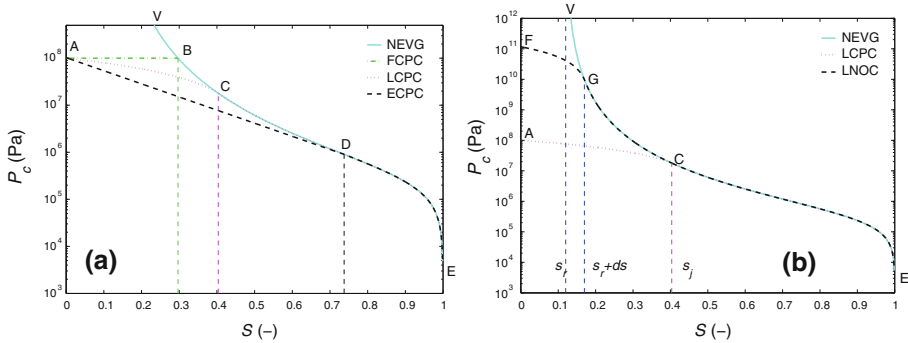*Note*: *CPC* capillary-pressure cap, *E* exponential, *F* flat, *L* linear, *NE* no extension, *VG* van Genuchten

Fig. 1 Comparison of capillary-pressure curves for host-rock unit tsw35 at Yucca Mountain (SNL 2007), where $\alpha = 3.38 \times 10^{-6}$ [Pa^{-1}], $m = 0.216$, and $S_r = 0.12$. **a** Comparison of the FCPC, ECPC, and LCPC with a CPC of 10^8 Pa. **b** The comparison of the original van Genuchten (NEVG) curve, with the LCPC and LNOC extensions. Three *vertical dashed lines* in **a** represent the transition saturation, S_j, respectively for FCPC, LCPC, and ECPC methods

$$P_c = \begin{cases} P_0 & S \leq S_j \\ \frac{1}{\alpha} \left(S_e^{-\frac{1}{m}} - 1 \right)^{\frac{1}{n}} & S \geq S_j \end{cases}, \tag{2}$$

where P_0 is the maximum capillary pressure. For this case, the transition saturation is

$$S_j = S_r + \left[1 + (\alpha P_0)^n \right]^{-m} (S_m - S_r). \tag{3}$$

2.2 Exponential Extension with Capillary-Pressure Cap (ECPC)

An exponential (ECPC) extension was introduced by Morel-Seytoux and Nimmo (1999) to modify Corey and van Genuchten capillary-pressure curves (curve ADE of Fig. 1a, Webb 2000),

$$P_c = \begin{cases} P_0 \exp(-\beta S) & S \leq S_j \\ \frac{1}{\alpha} \left(S_e^{-\frac{1}{m}} - 1 \right)^{\frac{1}{n}} & S \geq S_j \end{cases}, \tag{4}$$

where β is the slope of the capillary-pressure curve at S_j. Taking the first derivative of capillary pressure with respect to saturation yields

$$\frac{\mathrm{d}P_c}{\mathrm{d}S} = \begin{cases} -\beta P_0 \exp(-\beta S) & S \leq S_j \\ \frac{1}{\alpha(1-n)} \left(S_e^{-\frac{1}{m}} - 1 \right)^{-m} S_e^{-\frac{1+m}{m}} & S \geq S_j \end{cases}. \tag{5}$$

Variables S_j and β are determined through the solution of the following nonlinear equations (continuity of P_c and its first derivative):

$$\begin{aligned} P_0 \exp(-\beta S_j) &= \frac{1}{\alpha} \left(S_{ej}^{-\frac{1}{m}} - 1 \right)^{\frac{1}{n}}, \\ -\beta P_0 \exp(-\beta S_j) &= \frac{1}{\alpha(1-n)} \left(S_{ej}^{-\frac{1}{m}} - 1 \right)^{-m} S_{ej}^{-\frac{1+m}{m}}, \end{aligned} \tag{6}$$

where

$$S_{ej} = \frac{S_j - S_r}{S_m - S_r} \quad S_j > S_r. \tag{7}$$

Note that the original van Genuchten capillary pressure is defined in the range from S_r to S_m rather than that between 0 and 1. The transition saturation, S_j, is re-scaled as S_{ej} in the domain between S_r and S_m.

2.3 Linear Extension without Capillary-Pressure Cap (LNOC)

For a given $S_j > S_r$, the linear extension of the capillary-pressure curve is made in the dry region using the gradient at S_j. This method was introduced for numerical considerations; however, it does not address the need for a finite maximum capillary pressure (Nitao 1998; Finsterle 2002). Taking the first derivative of capillary pressure from Eq. 1 at S_j yields

$$\frac{dP_c(S_j)}{dS} = \frac{1}{\alpha(1-n)} \left(S_{ej}^{-\frac{1}{m}} - 1 \right)^{-m} S_{ej}^{-\frac{1+m}{m}}, \tag{8}$$

and the capillary pressure in the dry region is defined linearly

$$P_c = \begin{cases} P_c(S_j) - S\dfrac{dP_c(S_j)}{dS} & S \le S_j \\ \dfrac{1}{\alpha} \left(S_e^{-\frac{1}{m}} - 1 \right)^{\frac{1}{n}} & S \ge S_j \end{cases}. \tag{9}$$

LNOC extension is different from others (FCPC, LCPC, and ECPC) in that the maximum capillary pressure depends on S_j. That is, the maximum capillary pressure is not bounded; rather, it is a function of the transition saturation, S_j, and the first derivative of the capillary pressure, $dP_c(S_j)/dS$. LNOC is the default option in the NUFT code (Nitao 1998). The transition saturation is chosen as $S_j = S_r + 0.05(S_m - S_r)$.

2.4 Linear Extension with Capillary-Pressure Cap (LCPC)

A linear (LCPC) extension of the capillary-pressure curve was applied by Spycher et al. (2003) to avoid numerical difficulties associated with the extremely high capillary pressure. For a given CPC at zero saturation, the transition saturation can be calculated to ensure a smooth slope. For this case, the capillary pressure is

$$P_c = \begin{cases} P_0 - \beta S & S \le S_j \\ \dfrac{1}{\alpha} \left(S_e^{-\frac{1}{m}} - 1 \right)^{\frac{1}{n}} & S \ge S_j \end{cases}, \tag{10}$$

and the first derivative of P_c is

$$\frac{dP_c}{dS} = \begin{cases} -\beta & S \le S_j \\ \dfrac{1}{\alpha(1-n)} \left(S_e^{-\frac{1}{m}} - 1 \right)^{-m} S_e^{-\frac{1+m}{m}} & S \ge S_j \end{cases}. \tag{11}$$

The variable S_j and β are identified by solving the following nonlinear equations:

$$\begin{aligned} P_0 - \beta S_j &= \frac{1}{\alpha} \left(S_{ej}^{-\frac{1}{m}} - 1 \right)^{\frac{1}{n}}, \\ -\beta &= \frac{1}{\alpha(1-n)} \left(S_{ej}^{-\frac{1}{m}} - 1 \right)^{-m} S_{ej}^{-\frac{1+m}{m}}. \end{aligned} \tag{12}$$

3 The Thermal-Hydrologic Model

The MSTHM was developed to address thermal-hydrologic processes occurring at a scale of a few tens of centimeters around individual waste packages and emplacement drifts, and for heat flow at the multi-kilometer scale around the nuclear waste repository at Yucca Mountain (Buscheck et al. 2006). The MSTHM integrates the results of four families of submodels of various scales, dimensionality, and heat-source representation. Three of the submodel families represent thermal conduction at different scales, as well as thermal radiation in the emplacement drifts. The fourth submodel family, called the two-dimensional, line-averaged, drift-scale thermal-hydrologic (LDTH) submodel, represents thermal-hydrologic processes in the MSTHM. Contrary to thermal conduction/radiation models, the LDTH submodel results are sensitive to the capillary-pressure function; hence, we use the LDTH submodel (SNL 2007) to investigate the impact of various extensions with and without a CPC. In addition, a three-dimensional, thermal-hydrologic model has been developed to represent thermal-hydrologic behavior for the (DST) at Yucca Mountain. Descriptions of the test, including analyses of the experimental data, are provided by Birkholzer and Tsang (2000), Rutqvist et al. (2005), and Mukhopadhyay et al. (2007). In the thermal-hydrologic models, the fractured rock is represented as a dual-permeability system (Buscheck et al. 2002). The transport in the fracture continuum is further modified using the *active-fracture concept* (Liu et al. 1998). The thermal-hydrologic models describe mass and heat transport of two components (water and air) in two phases (liquid and gas) by advection, dispersion, thermal conduction, and thermal radiation. Simulations are conducted using the NUFT v3.0.1s code (Nitao 1998).

3.1 Governing Equations

The MSTHM solves the balance equations for water, air, and energy components in liquid, gas, and nondeformable solid phases (Buscheck et al. 2002). The mass balance equations for the water and air components in liquid and gas phases are

$$\frac{\partial}{\partial t} \sum_{\xi} \phi \rho_\xi S_\xi \omega_\xi^\zeta = -\sum_{\xi} \nabla \cdot \phi \rho_\xi S_\xi \left(\omega_\xi^\zeta \mathbf{v}_\xi + \mathbf{J}_\xi^\zeta \right), \quad \zeta = w, a, \ \xi = l, g, \qquad (13)$$

where t [s] is the time, ζ denotes the component (water or air), and ξ denotes the fluid phase (liquid or gas), ϕ [−] is the porosity, ρ_ξ [kg m^{-3}] is the phase density, S_ξ [−] is the saturation of phase ξ, ω_ξ^ζ [−] is the mass fraction of component ζ in phase ξ, $\mathbf{v}_\xi$ [m s^{-1}] is the advective phase velocity, and $\mathbf{J}_\xi^\zeta$ [m s^{-1}] is the combined diffusive and dispersive flux. The diffusive and dispersive flux term is described by a Fickian-type law

$$\mathbf{J}_\xi^\zeta = -\mathbf{D}_\xi^\zeta \nabla \omega_\xi^\zeta, \qquad (14)$$

and the advective flux is described by Darcy's Law

$$\phi S_\xi \mathbf{v}_\xi = -\frac{k_\xi (S_\xi)}{\mu_\xi} \left(\nabla P_\xi + \rho_\xi g \nabla z \right), \quad \xi = l, g, \qquad (15)$$

with $S_l + S_g = 1$ for the dual-phase system. The symbol $\mathbf{D}_\xi^\zeta$ [m^2 s^{-1}] denotes the combined diffusion and dispersion coefficient, k_ξ [m^2] is the permeability function, μ_ξ [Pa s] is phase viscosity, P_ξ [Pa] is phase pressure, and g [m s^{-2}] denotes the gravitational acceleration. The gas- and liquid-phase pressures are related by the capillary pressure

$$P_l = P_g - P_c, \tag{16}$$

where P_l and P_g are the liquid- and gas-phase pressure, and the capillary pressure P_c is defined by the modified van Genuchten relation (Liu et al. 1998)

$$P_c = \begin{cases} \text{LNOC|FCPC|ECPC|LCPC} & S \leq S_j \\ \frac{1}{\alpha}\left(S_e^{-\frac{\gamma}{m}} - 1\right)^{\frac{1}{n}} & S \geq S_j \end{cases}. \tag{17}$$

The parameter γ denotes the connectivity of the fracture network with zero for no connectivity and one for full connectivity. Note that γ always equals one in the matrix continuum. The relative permeability is given by

$$k_r = \begin{cases} 0 & S < S_r \\ S_e^{1-\frac{\gamma}{2}}\left[1 - \left(1 - S_e^{\frac{\gamma}{m}}\right)^m\right]^2 & S \geq S_r \end{cases}. \tag{18}$$

The definition of γ is opposite to that of Liu et al. (1998), and Eqs. 17 and 18 are adjusted accordingly. Figure 2 illustrates the relationship between the relative permeability and the capillary pressure modified using the LCPC and ECPC extensions. For example, the relation for the LCPC can be expressed as:

$$k_r = \begin{cases} 0 & S \leq S_r \\ \frac{P_0 - P_c - \beta S_r}{\beta(1-S_r)}\left\{1 - \left[1 - \left(\frac{P_0 - P_c - \beta S_r}{\beta(1-S_r)}\right)^{\frac{1}{m}}\right]^m\right\}^2 & S_r < S < S_j \\ \frac{\left\{1 - (\alpha P_c)^{n-1}[1+(\alpha P_c)^n]^{-m}\right\}^2}{[1+(\alpha P_c)^n]^{\frac{m}{2}}} & S \geq S_j \end{cases}. \tag{19}$$

Although capillary pressure is artificially modified in the dry region ($S < S_j$), relative permeability keeps the original form. The gas-phase permeability is assumed to be com-
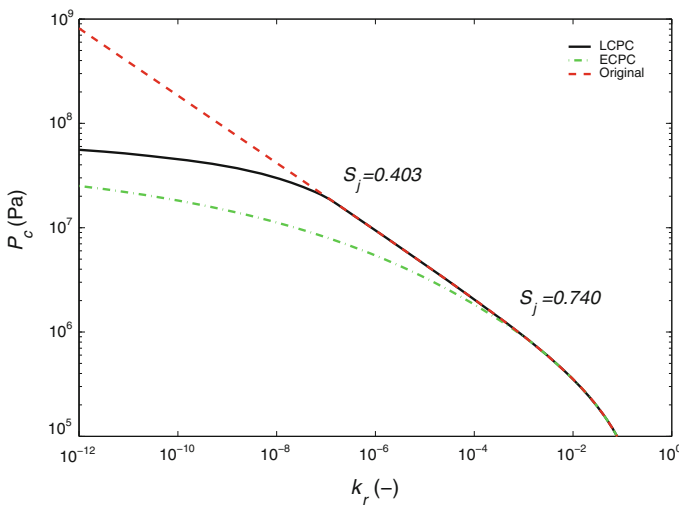

Fig. 2 Relationship between capillary pressure and relative permeability for the LCPC and ECPC extensions. $S_r = 0.12$, $\alpha = 3.38 \times 10^{-6}$ [Pa^{-1}], and $m = 0.216$

plementary to the liquid-phase permeability. In principle, the extension of capillary pressure is applied to both rock matrix and fractures. However, because the residual saturation in fractures is assumed to be zero, the calculated transition saturation, S_j, in fracture materials is also close to zero. Thus, the dry region of fracture materials is insignificantly narrow, and only LNOC should be used for fracture domain.

The energy balance equation is (Buscheck et al. 2002)

$$\frac{\partial}{\partial t}\left[\sum_{\xi}\phi\rho_\xi u_\xi S_\xi + (1-\phi)\rho_s c_p(T-T')\right] = -\sum_{\zeta}\sum_{\xi}\left[\nabla\cdot\phi h_\xi^\zeta \rho_\xi S_\xi\left(\omega_\xi^\zeta \mathbf{v}_\xi + \mathbf{J}_\xi^\zeta\right)\right]$$
$$+\nabla\cdot K\nabla T, \tag{20}$$

where T [°C] denotes the temperature, c_p [J kg^{-1} °C^{-1}] is the specific heat capacity of the solid phase, ρ_s [kg m^{-3}] is the solid density, u_ξ [J kg^{-1}] is the specific internal energy, h_ξ^ζ [J kg^{-1}] is the partial specific enthalpy, K [W m^{-1} °C^{-1}] is the thermal conductivity, and T' [°C] is a reference temperature. Heat is transported by thermal conduction, advective and diffusive heat fluxes, and radiative heat transfer in the drift open space. Radiative energy flux is calculated from Stefan-Boltzmann equation

$$Q = c(T_1^4 - T_2^4) \tag{21}$$

where T_1 is the absolute temperature of the radiator, T_2 is the absolute temperature of the receiver, and c is a coefficient defined by $c = AF\varepsilon\sigma$, where A is the area of the radiating surface element, F is the radiative view factor (Buscheck et al. 2002), ε is the emissivity, and σ is Stefan-Boltzmann constant.

Our model utilizes a dual-permeability approach in which the fracture and matrix systems are treated as two separate continua with a complete set of governing equations and computational grid for each continuum. Each continuum has coupling terms for mass and energy fluxes between two continua. These terms have the general form $q = a\kappa \Delta u/L$, where q is the flux of mass or energy per unit bulk volume, Δu is the difference in pressure or temperature across continua, and κ is a transfer coefficient (Buscheck et al. 2002).

3.2 Study Domains and Grids

The DST was designed to investigate in situ thermal-hydrologic processes at the scale of a single emplacement drift (Birkholzer and Tsang 2000; Rutqvist et al. 2005; Mukhopadhyay et al. 2007). Figure 3 shows the plan view of the physical system.

As shown in Figs. 4 and 5a, the cross section, orthogonal to the heater axis, of a three-dimensional model, utilizing a five-level nested mesh, was developed to represent *drift-scale* thermal-hydrologic behavior in the DST. The model domain covers the entire unsaturated flow region from ground surface to the water table and includes the detailed geometry of the heater drift. Grid-block sizes range from a few tens of centimeters around the heated drift to tens of meters in the far field. The conceptual model based on a dual-permeability representation of overlapping fracture and matrix continua, modified from traditional approach such that only a portion of connected fractures actively advect in liquid-phase (Liu et al. 1998; Birkholzer and Tsang 2000). In this study, we focus on the influence of the extension methods to the van Genuchten capillary-pressure function on simulated drift-scale thermal-hydrologic behavior.

Initial conditions for the thermal-hydrologic model were obtained by running the model for 10^6 years using constant boundary conditions at the ground surface and water table, and

Fig. 3 Plan view of the DST area (modified from SNL 2007)

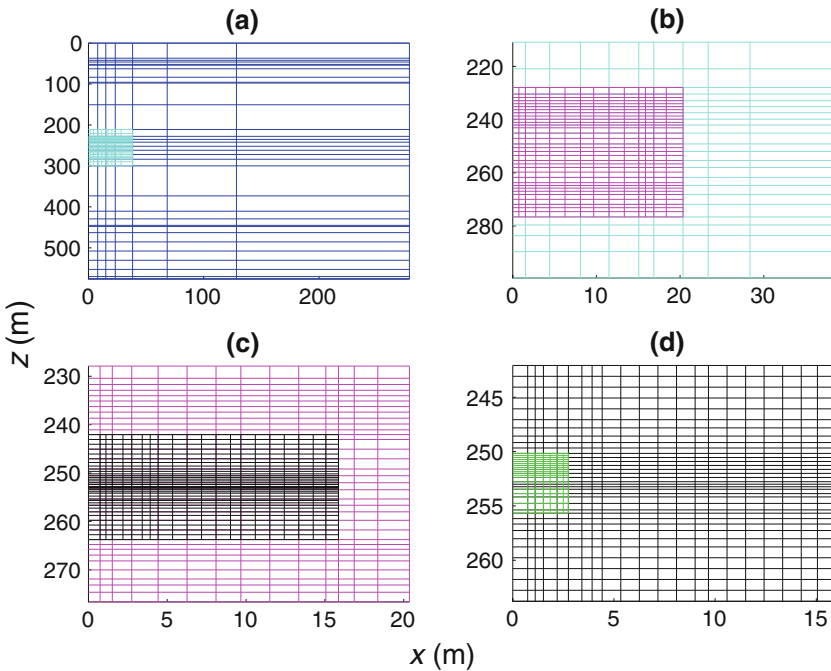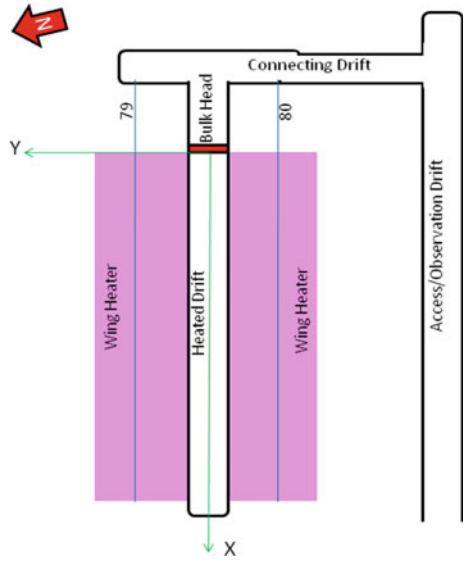**Fig. 4** The five-level nested mesh for the DST model at $y = 20$ m from the thermal bulkhead, which is roughly the midpoint along the longitudinal direction of the heater drift, including **a** Level 1 mesh, **b** Level 2 mesh, **c** Level 3 mesh, and **d** Level 4 mesh

net infiltration flux, resulting from rainfall and snowmelt. Both ground surface and water table are assumed to have the constant boundary conditions in pressure, temperature, air mass fraction, and relative humidity. The no-flow boundary conditions for both mass and
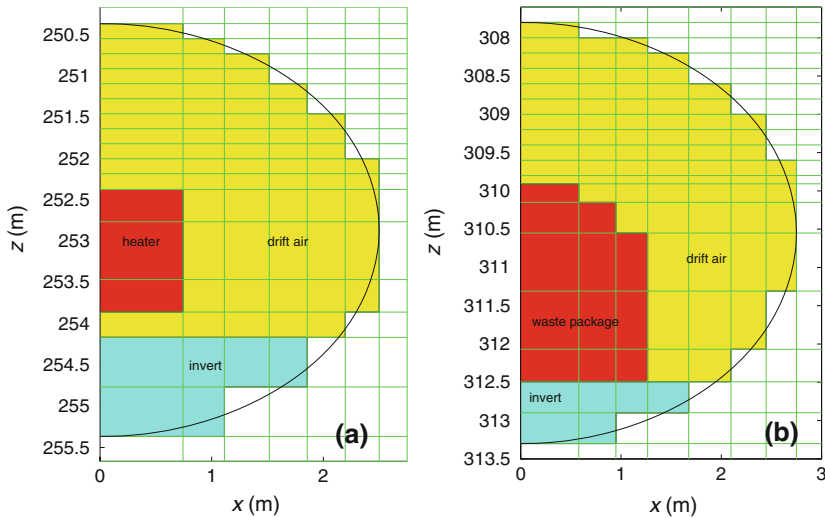
Fig. 5 **a** The Level 5 mesh of the region around the heated drift of the DST at $y = 20$ m from the thermal bulkhead. The *red* and *yellow zones* are heater and drift blocks, respectively. The *blue zone* is the invert at the bottom of the drift. **b** The mesh of the region around the emplacement drift in the LDTH submodel of the MSTHM (SNL 2007) at a typical location close to the repository center

energy are assumed horizontally (in x and y directions) since the model domain is extended by 1,000 m from the origin (center of the bulkhead).

3.3 System Parameters

The original calibrated van Genuchten relation is always applied over the saturation range from S_j to S_m, while between S_j and zero saturation, the appropriate extension is applied. The unsaturated zone hydrostratigraphy at Yucca Mountain consists of 39 welded- and nonwelded-tuff hydrostratigraphic units. The van Genuchten parameters, α and m, as well as residual and maximum saturations, were previously calibrated using iTOUGH (Finsterle 2002) for ambient conditions (Zhou et al. 2003); therefore, strictly speaking, these parameters are applicable between S_r and S_m. In order to extend the van Genuchten curves derived for the wet (ambient) region to the dry region, the four methods listed in Table 2 are applied. For a given hydrostratigraphic unit and maximum capillary pressure, S_j is a function of the extension method. S_j can be calculated for FCPC without an iterative process (Eq. 3), but should be numerically determined for ECPC and LCPC by solving nonlinear equations (Eqs. 6, 12). Transition saturations subject to a CPC of 10^8 Pa for the 39 hydrostratigraphic units are shown in Fig. 6. Blue fill represents the dry regions by linear (LCPC) extension, and the combined blue and green regions represent the dry regions by exponential (ECPC) extension. The green regions, with average width of 0.15, indicate that the exponential extension covers a wider saturation range (S_j is fairly high), while the linear (LCPC) extension minimizes the dry regions(S_j is lower). In general, it is preferred to maintain wider wet regions (low S_j) to rely preferentially on the calibrated $P_c(S)$ curves.

The transition saturation is a function of van Genuchten α, m, S_r, and S_m. In order to facilitate sensitivity analyses, the transition saturation is tabulated as a library for all hydrostratigraphic units as a function of van Genuchten α, m, and the maximum capillary pressure.
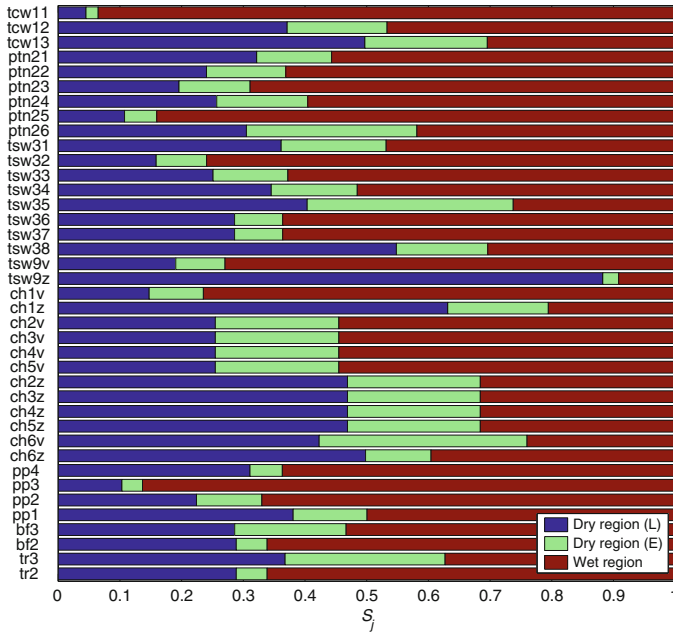
Fig. 6 Separation of wet and dry regions for the 39 hydrostratigraphic units at Yucca Mountain for a CPC of 10^8 Pa. The dry region for the LCPC extension is shown in *blue*. The dry regions for the ECPC extension are shown in *blue* and *green*. For drift-scale thermal-hydrologic behavior, the units of interest are the four host-rock units: tsw33, tsw34, tsw35, and tsw36
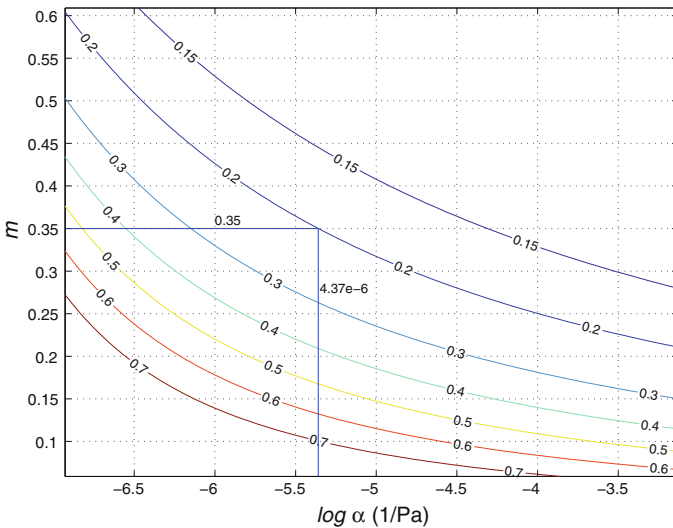

Fig. 7 LCPC S_j values as a function of van Genuchten α and m for the tsw35 hydrostratigraphic unit ($S_r = 0.12$) with a CPC of 10^8 Pa

For example, $S_j = 0.2$ when $\alpha = 4.36 \times 10^{-6}$ Pa^{-1} and $m = 0.35$ with a CPC of 10^8 Pa as shown in Fig. 7.

🌐 Springer

4 Model Results and Analyses

4.1 Comparing Measured and Simulated Results for the Drift-Scale Test

The data for the temperature and saturation from the DST have been collected and compiled to help understand drift-scale thermal-hydrologic processes in the proposed high-level nuclear waste repository at Yucca Mountain. Although interpretations of those data can be found in previous reports, this study represents the first systematic attempt to achieve better agreement between measured and simulated thermal-hydrologic behavior for sub-residual saturation.

4.1.1 Temperature Snapshots

Model results simulated with the NUFT code are compared to DST temperature measurements at different boreholes and times. Simulated temperature results are mapped onto all the available thermocouple sensors in Resistance Temperature Detector (RTD) boreholes. As shown in Figs. 8, 9, and 10, twelve snapshots of temperatures at Boreholes 137, 141, 158, 168, 79, and 80 compare DST data to models using the LNOC and LCPC extensions (see Table 3 for collar coordinates and borehole orientation). Note that simulations with the LCPC extensions were conducted with CPC values of 10^8 and 10^9 Pa. Because we found that the LCPC extension with a CPC of 10^8 Pa produces better agreement with measured temperatures and saturations, we decided to only present the results for a CPC of 10^8 Pa.
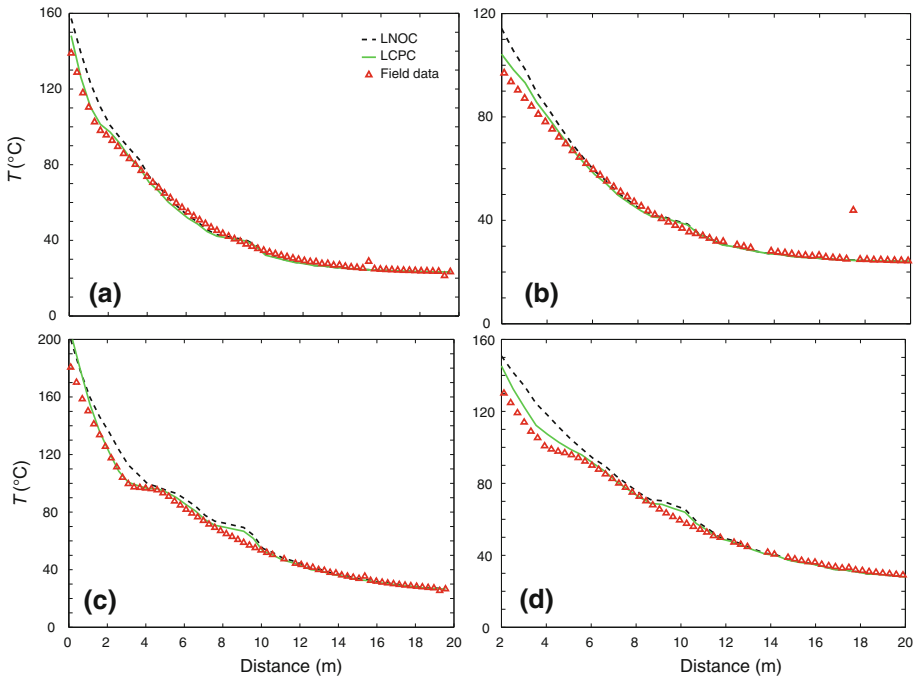

Fig. 8 Comparison of temperature snapshots at boreholes 137 and 141. **a** Borehole 137 at 365 days, **b** borehole 141 at 365 days, **c** borehole 137 at 730 days, and **d** borehole 141 at 730 days. The *y*-axis indicates the distance from the borehole collar at the drift wall
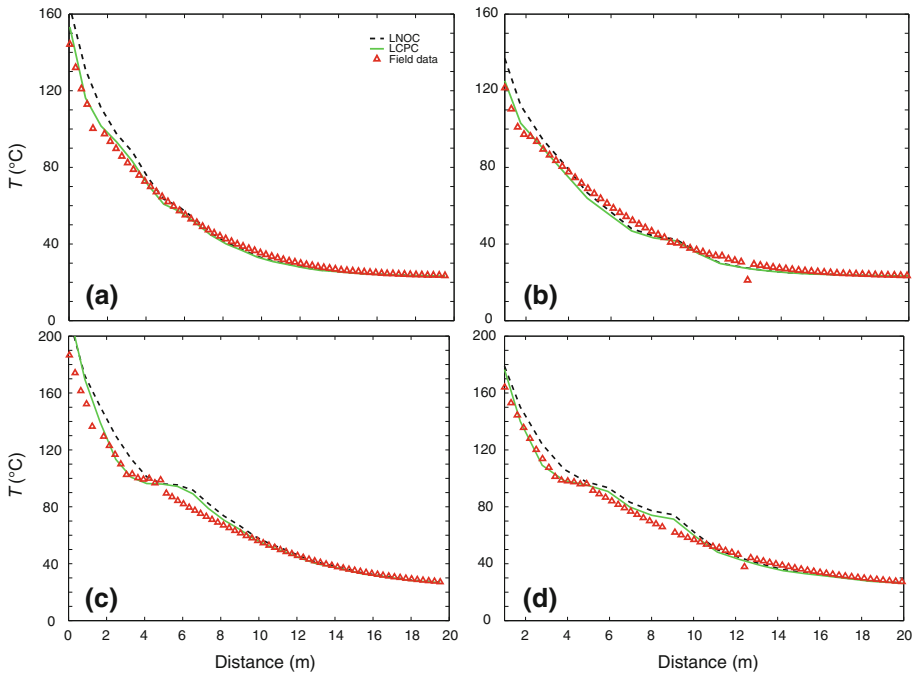
Fig. 9 Comparison of temperature snapshots at boreholes 158 and 168. **a** Borehole 158 at 365 days, **b** borehole 168 at 365 days, **c** borehole 158 at 730 days, and **d** borehole 168 at 730 days

Because models with FCPC, ECPC, and LCPC produce nearly identical temperature snapshots, only temperature snapshot from the LCPC model is plotted for an ease of comparison to LNOC results and field data. Temperature curves simulated using the LCPC extension with a CPC of 10^8 Pa (solid green curves) show better agreement with observed data than those simulated using the LNOC extension (dashed curves). Based on the root-mean-square error (RMSE) between simulated and measured temperatures, simulated temperatures using the LCPC extension are 16.7% closer to observed data than those using the LNOC extension. Figures 8, 9, and 10 illustrate how the LCPC extension results in better agreement between simulated and measured temperatures than the LNOC extension. As shown in Fig. 10a, when temperatures are below the boiling point, and wet (ambient) saturation conditions prevail, the LCPC and LNOC extensions yield identical simulated temperatures. On exceeding the boiling temperatures, the LCPC results in lower simulated temperatures than the LNOC extension, which more closely correspond to measured temperatures (Fig. 10b, c, d).

Heat pipes can result from the countercurrent flow of water vapor and liquid water between the boiling and condensation zones if the vapor and liquid fluxes are of sufficient magnitude. Because of the high efficiency of latent heat transport, the temperature gradient in the heat-pipe zone is minimal, resulting in nearly isothermal conditions (Birkholzer 2006). Capillary pressures play an important role in determining gas-phase flux from the hot end to the cool end of the heat pipe, and the liquid-phase flux back to the hot side. The absence of a CPC in the LNOC case causes a larger increase in vapor-pressure lowering than in the LCPC case. The larger vapor-pressure-lowering effect raises the boiling point, thereby inhibiting boiling and reducing the magnitude of vapor flow in the heat-pipe zone. Consequently, the smaller vapor flux in LNOC case results in less efficient heat transfer within the heat-pipe zone than
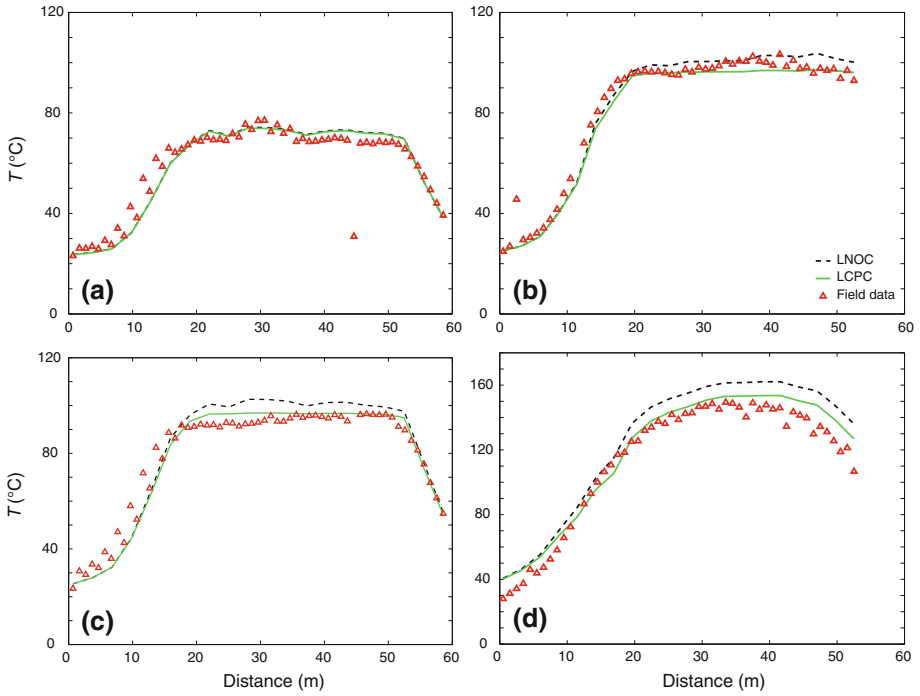
Fig. 10 Comparison of temperature snapshots at boreholes 79 and 80. **a** Borehole 80 at 175 days, **b** borehole 79 at 365 days, **c** borehole 80 at 365 days, and **d** borehole 79 at 1,650 days. The y-axis indicates the distance from the borehole collar at the drift wall

Table 3 Collar coordinates and borehole orientation

Borehole	x (m)	y (m)	z (m)	Orientation
67	−27.73	26.47	4.78	$x+$
79	9.46	−11.02	3.75	$y+$
80	−9.49	−11.06	3.23	$y+$
133	0.75	2.74	2.40	$z+$
134	0.73	2.73	1.60	$z-$
137	0.78	11.92	2.51	$z+$
141	0.76	11.89	−1.64	$z-$
158	0.76	22.85	2.57	$z+$
168	−0.07	31.93	2.45	$z+$

in the LCPC case. As shown in Fig. 11, the LCPC extension better represents the heat-pipe zone for two vertical (upward-oriented) boreholes.

4.1.2 Temperature Histories

For a given RTD sensor, the simulated borehole temperature history is compared with field measurements. As illustrated in Fig. 12, the temperature histories simulated with the LCPC extension show better agreement with the measured data.
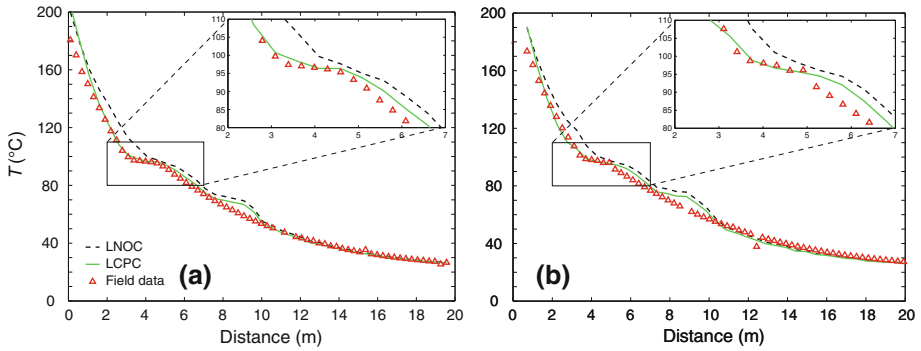
Fig. 11 Heat pipe at **a** borehole 137 and 730 days and **b** borehole 168 and 730 days. Both boreholes are oriented vertically upward
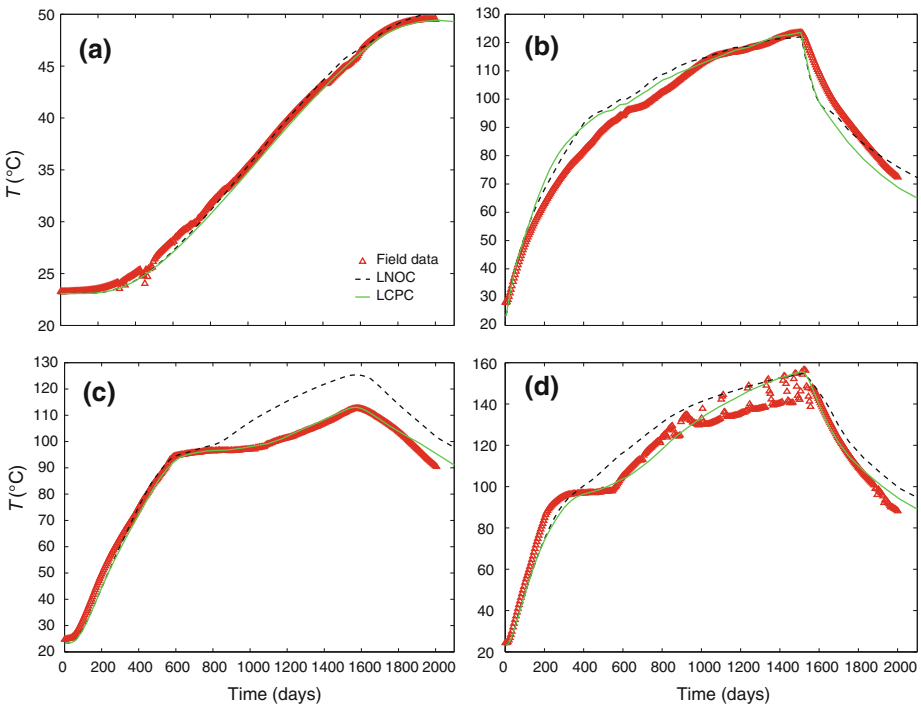

Fig. 12 Comparison of temperature history plots at **a** sensor 52 of borehole 133, **b** sensor 8 of borehole 134, **c** sensor 21 of borehole 79, and **d** sensor 29 of borehole 79

Simulated temperature histories for sub-boiling conditions are the same (e.g., Fig. 12a), regardless of extension method, because wet (ambient) saturation conditions prevail, and the respective extension methods have the same capillary-pressure representations for those conditions. Moreover, for sub-boiling conditions, heat flow is dominated by heat conduction. Thus, convection, which is influenced by hydrologic properties, does not noticeably affect temperatures for sub-boiling conditions. When temperatures reach or exceed the boiling point, phase change and convection exert dominant roles on temperature histories as shown in Fig. 12c, d. In the boiling zone, the LNOC extension results in larger capillary pressures
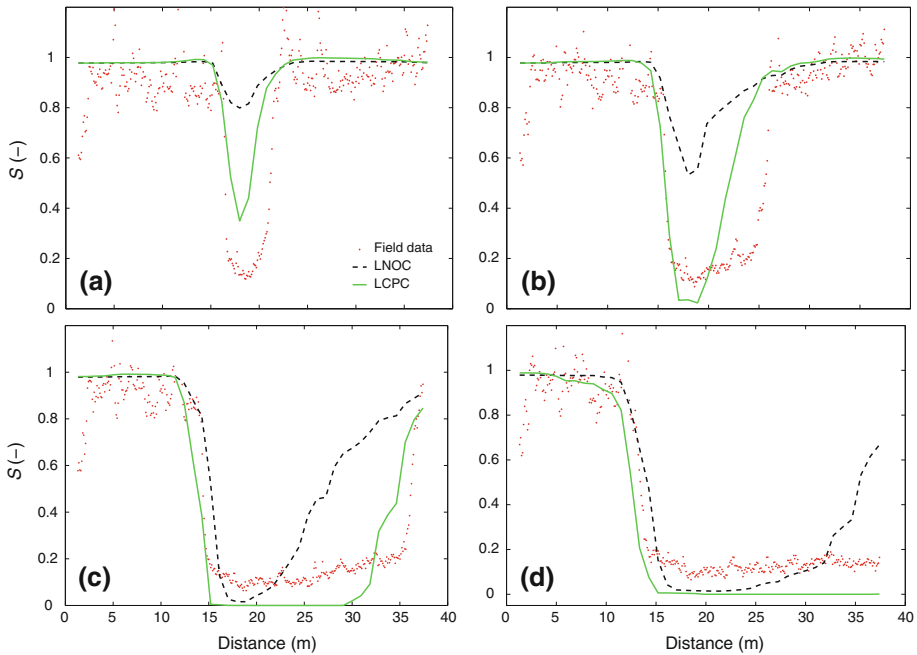
Fig. 13 Comparison of saturation snapshots at Borehole 67 for **a** 202, **b** 352, **c** 890, and **d** 1,888 days

than the LCPC extension, which increases the magnitude of the vapor-pressure lowering effect. The larger magnitude of vapor-pressure lowering in the LNOC case raises the boiling point, which inhibits boiling and reduces the magnitude of vapor flux and heat-transfer efficiency within the heat-pipe zone. The smaller magnitude of vapor-pressure lowering in the LCPC case results in a greater magnitude of vapor flux and higher heat-transfer efficiency within the heat-pipe zone, allowing temperatures to be maintained at the boiling point (96°C) for some period of time (Lin and Sun 2006). Because of the improved representation of boiling and heat transport in the heat-pipe zone, the LCPC case results in better agreement with measured temperatures, as shown in Fig. 12c, d.

4.1.3 Saturation Snapshots

Comparisons between measured and simulated saturation profiles are consistent with comparisons of measured and simulated temperatures discussed above. Larger capillary pressures in the LNOC case increase the magnitude of vapor-pressure lowering, which elevates the boiling point, inhibiting boiling and rock dryout. This explains why the dryout zone produced in the LNOC case is smaller than that produced in the LCPC case. As shown in Fig. 13c, d, the minimum saturation simulated in the LCPC case (as well as the LNOC case) is generally lower than the minimum saturation measured during the boiling period. This could be the result of uncertainty and heterogeneity of porosity, which is used to convert the measured water content to saturation.

4.2 Drift-Scale Thermal-Hydrologic Model Results

The model results presented in this subsection are generated using a two-dimensional drift-scale thermal-hydrologic model of a typical emplacement drift in the proposed high-level
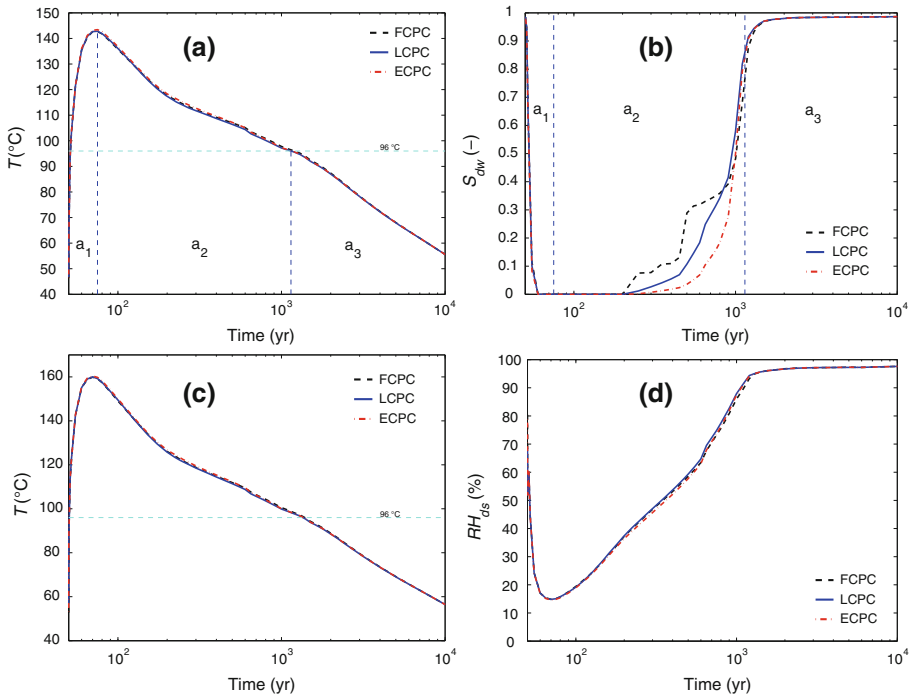
Fig. 14 Drift-wall temperature (**a**) and saturation (**b**), and drip-shield temperature (**c**) and relative humidity (**d**) at a location close to the repository center

nuclear waste repository at Yucca Mountain. This model is derived from the LDTH submodel of the MSTHM (Buscheck et al. 2006). A line-averaged heat source is calculated for the entire waste package inventory over the entire heated footprint of the repository. The LDTH model is a two-dimensional version, oriented perpendicular to the emplacement drifts, of the 3-D mountain-scale thermal-hydrologic system. Besides its specific purpose within the context of the MSTHM methodology, the LDTH submodel also serves as a useful stand-alone model, providing information and insight about drift-scale processes and parametric dependencies. Here, we investigate the influence of various capillary pressure extensions on simulated drift-wall temperature and saturation for a typical location close to the center of the Yucca Mountain repository. Earlier in this article, we demonstrated that a van Genuchten $P_c(S)$ curve extension with a CPC resulted in better agreement with temperatures and saturations measured in the DST than the one without a CPC, LNOC. Here, we compare flat (FCPC), linear (LCPC), and exponential (ECPC) extensions to the van Genuchten curve with a CPC of 10^8 Pa.

Figure 14 shows the drift-wall temperature and saturation, and drip-shield temperature and relative humidity, all of which are simulated using FCPC, LCPC, and ECPC extension methods at a typical location close to the repository center (SNL 2007). The time history is divided into heating (a_1) and cooling periods, with the cooling period further split into an above-boiling cooling (a_2) period and a sub-boiling cooling (a_3) period. Figure 14a, c, d shows that for all time, the selected extension method has a barely discernible (but insignificant) influence on simulated drift-wall and drip-shield temperature, as well as on drip-shield relative humidity. Only for drift-wall saturation, and only during a portion of the
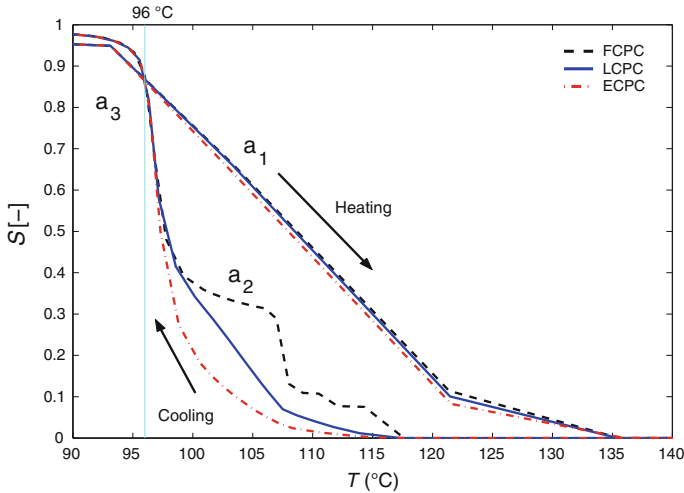
Fig. 15 Relation between drift-wall temperature and saturation at the location close to the repository center

above-boiling cooling (a_2) period, does the selected extension method have any discernable (but small) influence on the simulation (Fig. 14b). Moreover, during the latter portion of the above-boiling cooling (a_2) period, the simulated drift-wall saturations for all the three extension methods converge. Thus, as cool-down approaches the boiling point (and thereafter), the selected extension method has an insignificant influence on simulated drift-wall saturation.

For the above-boiling cooling (a_2) period, the FCPC extension results in slightly higher saturation, and the ECPC extension results in slightly lower saturation than the LCPC extension. Notice that the differences in simulated saturation only occur for dry conditions, with saturation values less than 0.4. For above-boiling, low-saturation conditions, rewetting is affected by vapor transport and condensation, while for higher saturation conditions, rewetting is dominated by liquid-phase flow, primarily driven by the local percolation flux (Buscheck et al. 2006). For low saturation, differences in saturation history reflect the distinct rates of rewetting resulting from capillary condensation. The higher values of capillary pressure in the FCPC case (see Fig. 1) cause a greater vapor-pressure lowering effect, resulting in faster rewetting by capillary condensation. The lower values of capillary pressure in the ECPC case cause a smaller vapor-pressure-lowering effect, resulting in slower rewetting by capillary condensation. Once saturation values exceed 0.4, rewetting is dominated by liquid-phase rewetting, which is controlled by the local percolation flux (Buscheck et al. 2006). Thus, rewetting to ambient (wet) saturation conditions is unaffected by the choice of extension method.

The relationship between drift-wall temperature T and saturation S is shown in Fig. 15. During both the heating (a_1) and sub-boiling cooling (a_3) periods, the T–S relations for the three extensions are identical. For reasons discussed earlier, during the above-boiling cooling (a_2) period, the FCPC and ECPC extensions result in faster and slower rewetting, respectively, than that resulting from the LCPC extension. Note that the influence of capillary condensation on vapor-phase rewetting begins at a temperature of about 117°C.

Because all the three extension methods with a CPC result in similar simulated thermal-hydrologic behavior for a typical location in the Yucca Mountain nuclear waste repository (virtually identical with respect to temperature and relative humidity), it is reasonable to consider computational efficiency to help select the preferred extension method.
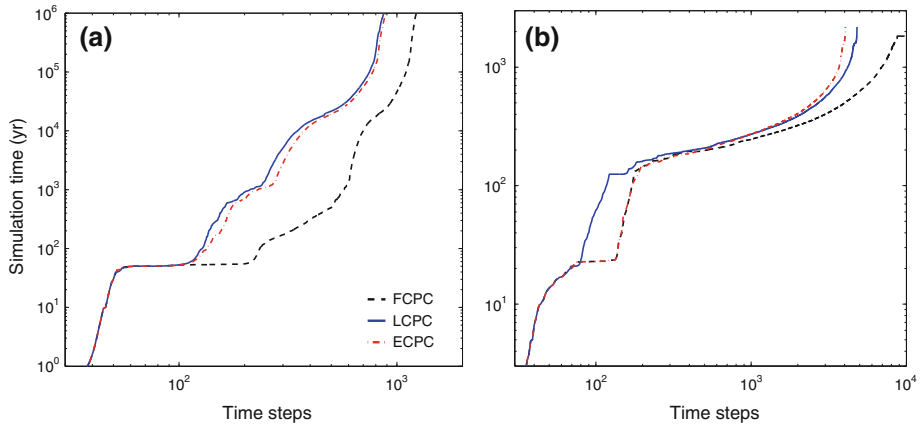
Fig. 16 Numerical performance of FCPC, LCPC, and ECPC extensions in **a** the two-dimensional drift-scale thermal-hydrologic model of a typical location in the Yucca Mountain repository and **b** the three-dimensional nested Drift-Scale Test (DST) model

Table 4 Comparison of root-mean-square error

Extension	175 days	365 days	730 days	1,096 days	1,500 days	1,650 days
FCPC	4.24	3.50	6.96	9.25	10.85	8.44
LCPC	4.21	3.51	7.00	9.27	10.86	8.44
ECPC	4.20	3.53	7.13	9.34	10.96	8.45
LNOC	5.14	4.88	7.46	9.36	10.82	12.50

4.3 Numerical Performance and Overall Comparison

We have demonstrated that an extension of the van Genuchten capillary-pressure curves with a CPC provides better agreement between the measured DST data and the simulated results than that provided by an extension without a CPC (see Figs. 8, 9, 10, 11, 12,13). More specifically, we showed that the LCPC extension results in better agreement with temperature and saturation measurements in the DST than that resulting from the LNOC extension. We also showed that all the three different extension methods with a CPC of 10^8 Pa result in essentially the same simulated thermal-hydrologic behavior at a typical location in the Yucca Mountain nuclear waste repository. Therefore, it is reasonable to choose an extension method on the basis of computational efficiency. To this end, we investigate the numerical performance of the FCPC, LCPC, and ECPC extensions.

Figure 16 compares computational efficiencies for the two-dimensional drift-scale thermal-hydrologic model of a typical location in the Yucca Mountain repository and for the DST model for the three extension methods. At early stages (corresponding to the pre-boiling period), there are no significant differences in terms of simulation speed. During the boiling and rewetting periods, the LCPC and ECPC extensions result in nearly equal simulation speeds, while the FCPC extension has a significantly slower speed. During the boiling period of the DST model, the LCPC extension results in faster simulation than the FCPC and ECPC extensions. However, during the rewetting period, the ECPC extension results in slightly more efficient simulation than the LCPC extension. It is noted that the simulation

using LNOC extension failed to reach the end of the simulation period for the DST model because of the unrealistically high capillary pressure, which causes rewetting to be too fast.

The RMSE between simulated and measured temperatures is calculated for all the available boreholes at six different times, as shown in Table 4. All the three extension methods with a CPC of 10^8 Pa result in better agreement with temperature data than the LNOC extension, which has no CPC. For 365, 730, 1,096, and 1,500 days, the FCPC extension yields a slightly lower RMSE compared to LCPC and ECPC. However, the marginal improvement in RSME does not warrant the additional computational expense of the FCPC extension. Therefore, we prefer the use of the LCPC extension to the van Genuchten capillary-pressure curves.

5 Conclusions

Applicability of the van Genuchten curves calibrated under ambient (wet) conditions to the strongly heat-driven (dry) conditions expected at the Yucca Mountain nuclear waste repository is addressed in this article; this question had not been previously addressed in great detail. In this article, various mathematical expressions are used to describe capillary pressure as a function of saturation under strongly heat-driven conditions, and the concept of transition saturation is used to divide dry and wet regions. The van Genuchten curves calibrated for ambient conditions are used in the wet region while synthetic extensions are used in the dry region. The extension of capillary-pressure curves not only eliminates the singularity at residual saturation, but better reflects the fact that capillary pressure should be capped at some finite, physically reasonable value (i.e., less than the rock yield stress).

Measured temperature and saturation data in the DST are used to test various extension methods with and without CPCs. Agreements between simulated and measured values of both temperature and saturation are compared across all extension methods. It is found that all the three extension methods with a CPC of 10^8 Pa result in significantly better agreement between simulated and measured values than that resulting from an extension method with no CPC. Moreover, the RMSE between the simulated and measured temperature is similar for the three extensions with CPC, and is significantly smaller than the RMSE for the extension method with no CPC.

The three transition methods with a CPC of 10^8 Pa are applied to a two-dimensional, drift-scale thermal-hydrologic model of a typical location close to the center of the Yucca Mountain repository. All the three extension methods result in essentially identical simulations of drift-wall and drip-shield temperature, as well as drip-shield relative humidity. With respect to liquid saturation at the emplacement drift wall, the three transition methods result in the same simulated dryout behavior, and similar rewetting behavior, with the minor exception of very dry conditions, when capillary condensation dominates rewetting behavior. Therefore, for extensions with a CPC of 10^8 Pa, the selected extension method has an insignificant influence on simulated drift-scale thermal-hydrologic behavior for a typical location in the Yucca Mountain repository. Thus, the selection of a preferred extension method can be based on (1) computational performance and (2) the extent to which the van Genuchten curves, calibrated for ambient (wet) conditions, are utilized. The transition saturation of the LCPC extension is much smaller than that of the ECPC; thus, the LCPC extension utilizes a greater saturation range of the van Genuchten curves than the ECPC extension. For this reason, the LCPC extension is preferred over the ECPC extension. The FCPC extension is found to be much more computationally expensive than either the LCPC or ECPC extensions. For this reason, the LCPC extension is preferred over the FCPC extension.

In this article, we conducted numerical experiments using various extension methods to the van Genuchten capillary-pressure function and demonstrated better agreement with the measured data from the DST, and no undue computational expense, when using the linear (LCPC) extension method with a CPC of 10^8 Pa. It is acknowledged that other parameters not addressed by this study may also affect thermal-hydrologic behavior. Although this article is limited to the study of the impact of capillary pressure curves, the mathematical models of the extended capillary-pressure curves can be applied to other thermal-hydrologic problems under heat-driven conditions. Some assumptions, such as the maximum capillary pressure (10^8 Pa) at zero saturation do not reduce the generality of the model concept, and alternative assumptions could be incorporated as needed (e.g., a CPC of 10^9 Pa yielded poorer model fits to data and was not presented in this study). Numerically and physically, there must be a CPC when saturation approaches zero. For a given rock material, this cap value can determine the transition saturation and thermal-hydrologic behavior in the dry region.

References

Birkholzer, J.T.: Estimating liquid fluxes in thermally perturbed fractured rock using measured temperature profiles. J. Hydrol. **327**, 496–515 (2006)

Birkholzer, J.T., Tsang, Y.W.: Modeling the thermal-hydrologic processes in a large-scale underground heater test in partially saturated fractured tuff. Water Resour. Res. **36**(6), 1431–1447 (2000)

Brooks, R.H., Corey, A.T.: Properties of porous media affecting fluid flow. J. Irrig. Drain. Div. Am. Soc. Civ. Eng. **92**, 61–87 (1996)

Buscheck, T.A., Rosenberg, N.D., Gansemer, J., Sun, Y.: Thermohydrologic behavior at an underground nuclear waste repository. Water Resour. Res. **38**(3), 1431–1447 (2002)

Buscheck, T.A., Sun, Y., Hao, Y.: Multiscale thermohydrologic model supporting the license application for the Yucca Mountain Repository, American Nuclear Society, La Grange Park, IL. In: Proceedings 2006 International High-Level Radioactive Waste Management Conference, Las Vegas, 30 April–4 May 2006

Campbell, G.S.: A simple method for determining unsaturated conductivity from moisture retention data. Soil Sci. **117**, 311–314 (1974)

Campbell, G.S., Shiozawa, S.: Prediction of hydraulic properties of soils using particle-size distribution and bulk density data. In: International Workshop on Indirect Methods for Estimating the Hydraulic Properties of Unsaturated Soils, University of California, Riverside, CA (1992)

Fayer, M.J., Simmon, C.S.: Modified soil water retention functions for all matric suctions. Water Resour. Res. **31**(5), 1233–1238 (1995)

Finsterle, S.: iTOUGH Command Reference. Lawrence Berkeley National Laboratory, LBNL-40041, Berkeley (2002)

Flint, L.E.: Characterization of hydrogeologic units using matrix properties, Yucca Mountain, Nevada, U.S. Geological Survey Water Resources Investigations Report, 98–4243, 64 pp (1998)

Glascoe, L.G., Buscheck, T.A., Gansemer, J., Sun, Y., Lee, K.: Multiscale thermohydrologic model analyses of heterogeneity and thermal-loading factors for a proposed nuclear waste repository. Nucl. Technol. **48**, 125–137 (2004)

Khlosi, M., Cornelis, W.M., Gabriels, D., Sin, G.: Simple modification to describe the soil water retention curve between saturation and oven dryness. Water Resour. Res. **42**(12), W11501 (2006). doi:10.1029/2005WR004699

Kolditz, O., De Jonge, J.: Non-isothermal two-phase flow in low-permeable porous media. Comput. Mech. **33**, 345–364 (2004)

Kosugi, K.: General model for unsaturated hydraulic conductivity for soils with log-normal pore-size distribution. Soil Sci. Soc. Am. J. **63**, 270–277 (1999)

Li, K., Horne, R.N.: Steam-water capillary pressure. In: Proceedings of the World Geothermal Congress, Antalya, Turkey, 24–29 April 2005

Lin, W., Sun, Y.: Thermal hydrological processes in the drift-scale thermal test at Yucca Mountain, Nevada. Lawrence Livermore National Laboratory, California, UCRL-JRNL-219897 (2006)

Liu, H.H., Doughty, C., Bodvarsson, G.S.: An active fracture model for unsaturated flow and transport in fractured rocks. Water Resour. Res. **34**(10), 2633–2646 (1988)

Luckner, L., van Genuchten, M.T.H., Nielson, D.R.: A consistent set of parametric models for the two-phase flow of immiscible fluids in the subsurface. Water Resour. Res. **25**, 2187–2193 (1989)

Morel-Seytoux, H.J., Nimmo, J.R.: Soil water retention and maximum capillary drive from saturation to oven dryness. Water Resour. Res. **35**(7), 2031–2041 (1999)

Mukhopadhyay, S., Tsang, Y., Birkholzer, J.T.: Estimation of field-scale thermal conductivities of unsaturated rock from *in situ* temperature data. Water Resour. Res. **43**, W09418 (2007). doi:10.1029/2006WR005283

Nieber, J.L., Dautov, R.Z., Egorov, A.G., Sheshukov, A.Y.: Dynamic capillary pressure mechanism for instability in gravity-driven flows: review and extension to very dry conditions. Transp. Porous Med. **58**, 147–172 (2005)

Nitao, J.J.: User's Manual for the USNT Module of the NUFT Code, Version 2 (NP-phase, NC-component, thermal). Lawrence Livermore National Laboratory, UCRL-MA-130653 (1998)

Nitao, J.J., Bear, J.: Potentials and their role in transport in porous media. Water Resour. Res. **32**(2), 225–250 (1996)

Ross, P.J., Williams, J., Bristow, K.L.: Equation for extending water-retention curves to dryness. Soil Sci. Soc. Am. J. **55**, 923–927 (1991)

Rossi, C., Nimmo, J.R.: Modeling of soil water retention from saturation to oven dryness. Water Resour. Res. **30**(3), 701–708 (1994)

Rutqvist, J., Barr, D., Datta, R., Gens, A., Millard, A., Olivella, S., Tsang, C.-F., Tsang, Y.: Coupled thermal-hydrological-mechanical analyses of the Yucca Mountain Drift Scale Test–Comparison of field measurements to predictions of four different numerical models. Int. J. Rock Mech. Min. Sci. **42**, 680–697 (2005)

Sandia National Laboratories (SNL): Multiscale Thermohydrologic Model. ANL-EBS-000049 REV 03 AD 01, Las Vagas, Nevada (2007)

Spycher, N.F., Sonnenthal, E.L., Apps, J.A.: Fluid flow and reactive transport around potential nuclear waste emplacement tunnels at Yucca Mountain, Nevada. J. Contam. Hydrol. **62–63**, 653–673 (2003)

Sun, Y., Buscheck, T.A., Hao, Y.: Influence of hydrologic heterogeneity on thermal-hydrologic conditions in emplacement drifts, American Nuclear Society, La Grange Park, IL. In: Proceedings 2006 International High-Level Radioactive Waste Management Conference, Las Vegas, 30 April–4 May 2006

van Genuchten, M.T.H.: A closed-form equation for predicting the hydraulic conductivity of unsaturated soils. Soil Sci. Soc. Am. J. **44**, 892–898 (1980)

Webb, S.W.: A simple extension of two-phase characteristic curves to include the dry region. Water Resour. Res. **36**(6), 1425–1430 (2000)

Zhou, Q., Liu, H.H., Bodvarsson, G.S., Oldenburg, C.M.: Flow and transport in unsaturated fractured rock: effect of multiscale heterogeneity of hydrogeologic properties. J. Contam. Hydrol. **60**, 1–30 (2003)